Scilight

Bioelectrochemical Systems and Applications

https://www.sciltp.com/journals/bsa

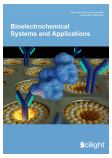

Article

Fabrication of A Robust Low-Cost High Performance Stainless Steel-Based Polypyrrole Anode for Microbial Fuel Cells

Jayesh M. Sonawane [1,*], Isha Kohli [2], R. K. Singh Raman [2], Prakash C. Ghosh [3] and Samuel Adeloju [4,*]

[1] Department of Microbiology, University of Massachusetts Amherst, Morrill IV N Science Center, Amherst, MA 01003, USA
[2] Department of Mechanical and Aerospace Engineering, Clayton Campus, Monash University, Clayton, VIC 3800, Australia
[3] Department of Energy Science and Engineering, Indian Institute of Technology Bombay, Mumbai 400076, India
[4] School of Chemistry, Clayton Campus, Monash University, Clayton, VIC 3800, Australia
* Correspondence: jay1iisc@gmail.com (J.M.S.); sam.adeloju@monash.edu (S.A.)

How To Cite: Sonawane, J.M.; Kohli, I.; Raman S.R.K.; et al. Fabrication of A Robust Low-Cost High Performance Stainless Steel-Based Polypyrrole Anode for Microbial Fuel Cells. *Bioelectrochemical Systems and Applications* **2025**, *1*(1), 3.

Received: 2 February 2025
Revised: 1 September 2025
Accepted: 25 September 2025
Published: 1 October 2025

Abstract: The use of stainless steel (SS) as an anode in a microbial fuel cell (MFC) suffers from significant limitations, such as poor biocompatibility, high activation overpotential, high charge transfer resistance, poor corrosion resistance, and its hydrophobic nature can hinder electron transfer. In this study, we present a robust approach for producing a low-cost, durable and biocompatible polyprrole (PPy) coating on a stainless plate (SS-P) anode for high performance MFC in harsh environments. The established galvanostatic polymerisation conditions produced PPy/SS-P anodes with improved surface area, enhanced electron transfer and good biocompatibility for enhanced MFC performance. Optimum PPy coating on the SS-P was achieved with an applied constant current density of 2.5 mA cm^{-2} for 15 min in a 0.7 M L-(+)-Tartaric acid solution, which contained 0.4 M Py. The effective formation of the PPy film on the SS-P was confirmed by chronopotentiometry and Fourier transform infrared (FTIR) spectroscopy. The nature of the PPy coating and its degree of hydrophilicity were investigated by contact angle measurements. It was found, for the first time, that this coating can transition from hydrophobic to hydrophilic upon exposure to an aqueous solution. This had a significant influence on the integrity and performance of the PPy coating when utilised for MFC. Also, in-depth analytical characterization of the PPy/SS-P was conducted by 3D profilometry and time-dependent electrochemical spectroscopy to provide insights into the nature and durability of the coatings. The subsequent utilization of the PPy/SS-P anodes in a single-chamber MFC gave a much lower open circuit voltage (OCV_{max}) of 355 ± 33 mV and 624 ± 47 mV for the first and second cycles, compared to 608 ± 32 mV and 664 ± 27 mV obtained for the SS-P anode. Also, the j_{max} of 0.027 ± 0.002 mA cm^{-2} and a P_{max} of 0.020 ± 0.009 mW cm^{-2} obtained with the PPy/SS-P anode were much higher than with the SS-P anode, which gave j_{max} of 0.0012 ± 0.0008 mA cm^{-2} and P_{max} of 0.010 ± 0.003 mW cm^{-2}. Furthermore, a 3-fold increase in electricity production was achieved during the startup phase with the PPy/SS-P anode, but such an increase was not realised with the SS-P anode. The proposed PPy/SS-P anode, therefore, offers a great promise for use as a low-cost anode in MFC.

Keywords: stainless steel; polypyrrole; galvanostatic polymerisation; high-performance anode; biomass growth; hydrophilicity; microbial fuel cell

1. Introduction

The breakdown of organic matter by electrogenic bacterial communities within the anode chamber is critical for generating electricity in a microbial fuel cell (MFC). For this reason, it is extremely important that the chosen anode is capable of achieving high performance under a chosen operating condition [1–5]. More specifically, it is necessary that the chosen anode material has a high biocompatibility [6–9], high chemical stability [6,10], high corrosion resistance to various wastewaters [2,6,11,12], low charge transfer resistance (R_{ct}) [9,13], and low activation overpotential [14]. Beyond these factors, the ability of the anode material to support microbial growth and facilitate electron transfer is critical to the overall performance of the MFC. In this regard, preference is usually given to anodes with hydrophilic surfaces that can achieve low charge transfer resistance, facilitate strong microbial growth/adhesion and have good biocompatibility [15–17].

Despite earlier assertions that stainless steel (SS) is a favorable anode for constructing high-performance MFCs [1,18–20], it has since been realised that SS exhibits several intrinsic properties that can limit its use for large-scale MFC construction. These limitations include its poor biocompatibility, which often leads to the formation of poor electrogenic bacterial biofilm, rendering it less effective for use in MFC [21]. Furthermore, SS has a high activation overpotential, a high charge transfer resistance, poor corrosion resistance in complex liquid media and it is hydrophobic in nature. However, it is possible to overcome these limitations by coating SS with a conductive polymer such as polyaniline, PPy, and polythiophene [9,22–25]. These polymers enhance the surface properties of anodes by increasing surface area, improving electrical conductivity, and producing a porous structure. Furthermore, these polymers have been found to amplify biofilm thickness and enhance bacterial attachment to the surface [26,27].

While polyaniline has been more widely used for coating stainless steel [28–31], there has been relatively few uses of PPy coatings on SS [22,32]. In one study, Wu et al. [9] developed a PPy/sargassum-activated carbon-modified SS by electrochemical polymerization of pyrrole on SS wool and achieved a P_{max} of 45.2 W m^{-3} with the anode. In another study [31], a j_{max} of 0.187 mW cm^{-2} was achieved with a PPy-coated SS wool anode compared with the 0.127 mW cm^{-2} obtained with a pristine SS. PPy-coated SS-P was also used to study the electrochemical kinetics of MFCs, and excellent biocompatibility for electrogenic bacteria was achieved [31,33]. In general, SS anodes coated with PPy often display low R_{ct}, high exchange current densities (j_o), high electrical conductivities, and high biocompatibilities that are necessary for achieving high MFC performance [34]. Some of the other reported uses of PPy-coating on other substrates for electricity generation in MFCs include PPy/reduced graphene oxide (rGO) composites [35], polyurethane/graphite/PPy composite [36], PPy hydrogels/carbon nanotubes composite [24], MnO_2/PPy composite-modified anode [37], PPy-coated Carbon Nanofiber [38] and PPy-coated CNT composite [39].

The PPy coatings used in many of the above studies were achieved by either chemical or electrochemical polymerization. Nonetheless, it is now well accepted that the latter enables much better control of the coating thickness and high reproducibility. However, the conditions used for electropolymerization of Py on a chosen substrate can significantly affect the nature and quality of the resulting PPy coating. Factors such as the type of electropolymerization mode, Py concentration, and the chosen polymerization time can directly affect the nature of the PPy coating and its performance, as well as its kinetics and longevity. Therefore, a comprehensive understanding of the long-term durability of PPy coatings and the fundamental mechanisms or factors influencing coating nature and degradation is necessary for the successful deployment of PPy/SS-P anodes for sustainable use in MFCs. Also, for the PPy coatings to be more resilient in harsh and complicated media, such as wastewaters and landfill leachates, the optimum coating thickness for each media must be determined.

In this study, we aim to investigate the durability of PPy coatings generated by galvanostatic polymerisation of pyrrole on SS-P and assess its suitability as an anode for MFCs, with a particular focus on identifying the optimum coating thickness required to enhance stability and performance in aggressive environments such as wastewaters and landfill leachates. Furthermore, as the startup and efficiency of an MFC are known to be significantly influenced by the performance and structure of the anode, our goal is to increase the efficiency of electricity production by modifying the SS-P anode with the best structured PPy coating. We anticipate that the durability and functional stability of PPy coatings on the SS-Ps can be significantly improved by elucidating the nature and behaviour of the coating before and after exposure to aggressive media. Therefore, in order to develop durable PPy/SS-P anodes for high-performance MFCs, various electrochemical testing and surface characterisation will be conducted. To ensure coating integrity and reliability, a galvanostatic polymerization approach was used to produce durable and highly reproducible PPy coatings. The integrity of the coating was further assured by careful investigation of the influence of L-(+)-Tartaric acid and Py concentrations on the nature of the coating formed on SS-304 plates and, hence, to establish the optimum conditions for the formation of the

durable and well-structured PPy coating. Furthermore, a detailed understanding of the nature and durability of the coatings was obtained by conducting an in-depth analytical characterization of the PPy coatings by contact angle measurements, Fourier-transformed infrared spectroscopy, 3D profilometry, and time-dependent electrochemical spectroscopy. To our knowledge, no similar detailed systematic investigation of durable PPy coatings on SS has been previously reported. Furthermore, to demonstrate the effectiveness of the coatings, we utilized the optimized PPy/SS-P anode in a MFC with M9 media+4% landfill leachate. We consequently evaluated the MFC performance in terms of voltage and current generation for a short duration to gain an understanding of the effect of the PPy coating on the MFC startup.

2. Materials and Methods

2.1. Electrode Preparation

A three-electrode setup was used to produce PPy coatings on SS plates (SS-Ps). The austenitic stainless steel **(**SS-304) plate was purchased from a local shop (Mumbai, Maharashtra, India). The SS-Ps used as a working electrode have a dimension of 1 × 1.5 × 0.1 cm and were polished with sandpaper of successive grit sizes of 320 to 1200. After polishing, the SS-Ps were ultrasonicated in acetone to degrease before coating with PPy by electropolymerization. A miniature Ag/AgCl reference electrode (RRPEAGCL), 3.43 mm dia, 74 mm length (Pine Research Instrumentation, Durham, USA) was used for voltage measurement and a platinum electrode was used as the counter electrode. A BiologicVMP3 potentiostat (BioLogic, Claix, France) was used for all electrochemical experiments. EC-Lab software was fitted with a potentiostat for the operation and analysis of the data obtained. Prior to commencing polymerization, all the solutions were purged with nitrogen gas for 10 min.

2.2. Electropolymerisation of Polypyrrole (PPy)

A reagent grade pyrrole and L-(+)-Tartaric acid (Sigma-Aldrich, Melbourne, Australia) were used for the electropolymerization on SS-Ps. The synthesis of PPy was achieved by galvanostatic polymerization, which involved the application of a constant current density of 2.5 mA cm^{-2} in aqueous solutions that contained Py. To establish the best conditions, the PPy film was synthesized with 0.1 M Py with varying concentrations of L-(+)-Tartaric acid within 0.1 and 0.7 M. Consequently, the L-(+)-Tartaric acid concentration, which gave the lowest activation and stabilizing potentials, was chosen as optimum for the synthesis of PPy as the resulting coating is most conductive and has the lowest R_{ct}. Also, while keeping the optimum L-(+)-Tartaric acid concentration constant, the Py concentration was varied within 0.1 and 0.5 M to determine the optimum Py concentration. After growing the PPy film for 15 min, the chronopotentiograms were analyzed to identify the lowest stabilization potential, which is indicative of the highest film conductivity for each condition. Scheme 1 outlines the methodology for the electrochemical synthesis of the PPy/SS-P anode and its exploration for use in MFCs.

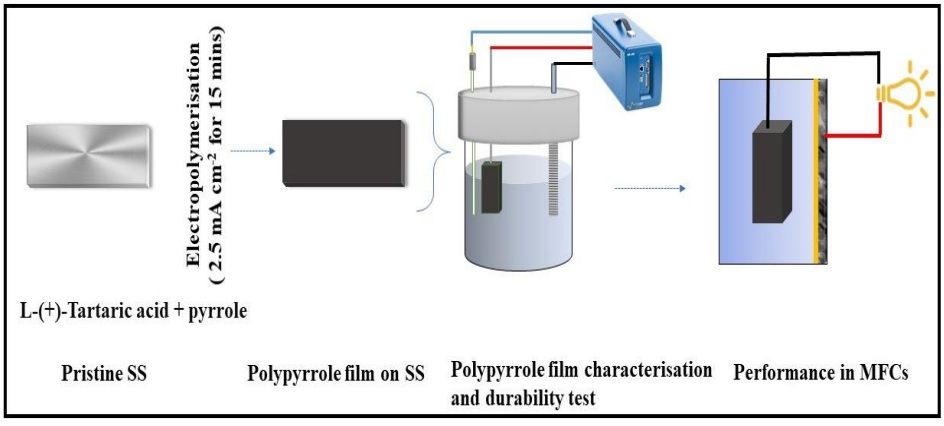

Scheme 1. Overall schematic of the process for coating of SS-P with PPy by galvanostatic polymerization of Py, electrochemical characterization and the use of PPy/SS-P as an anode in MFCs.

2.3. Surface Profilometry and Contact Angle Measurement

An InfiniteFocus microscope (Alicona, Raaba/Graz, Austria) was used to characterize the surface properties of the PPy films. Images were taken at different magnifications ranging from 10× to 50×. CAD/CAM suite (Alicona, Raaba/Graz, Austria) was used to analyze the surface profile of the PPy films. The sessile drop technique on a telephoto goniometer C60 (USA Kino Industry Co. Ltd., Norcross, GA, USA) was used to measure the water

contact angle of the PPy films at ambient temperature (19 °C) and 40% relative humidity. Three separate samples were analysed to ensure the reproducibility of the results.

2.4. Fourier Transform Infrared Spectroscopy (FTIR)

FTIR technique was used to study observable changes in the spectra obtained for the PPy/SS-Ps. FTIR spectrometer Vertex 80 (Bruker Optics, Billerica, MS, USA) was used to record the FTIR spectra of SS-P and PPy/SS-P. The attenuated total reflectance method was used to obtain the FTIR spectra with a 4 cm^{-1} resolution. The wavenumbers were kept within the range of 4000–650 cm^{-1}. After careful baseline corrections, the FTIR peaks were identified with Opus software (Bruker Corporation, Billerica, MA, USA).

2.5. Fabrication of the Cathode

The air cathodes used in this study were fabricated by using a previously reported method [30,31]. Briefly, 20 wt % platinized carbon Vulcan XC-72 (Sigma-Aldrich, Sydney, Australia) was used for coating on carbon paper. Nafion solution (5%) was used as a binder (Sigma-Aldrich, Sydney, Australia). The Nafion solution was mixed with the Pt powder in isopropyl alcohol, and the resulting Pt ink was ultrasonicated with a probe sonicator for at least 15 min. The ink was coated on a 12 × 10 cm carbon paper (GDS 210, CeTech, Taichung, Taiwan) to achieve 0.5 mg cm^{-2} loading. Utmost care was taken to ensure uniform loading of Pt over the surface of the carbon paper. To ensure proper drying, the coated carbon papers were placed in the oven for six hours at 60 °C. After drying, a monolayer of 5% Nafion solution was applied and placed in an oven for 15 min.

Consequently, the coated carbon papers were hotpressed with a Carver hotpress (Carver, Inc, Wabash, IN, USA) on the Nafion membrane (NRE-212) under a 1200 kg at 140 °C for 3 min.

Hotpressed electrodes were cut to 3 × 2.5 cm portions. The cathodes were then sandwiched in an aluminum mesh (acts as a cathode current collector) and acrylic flange in the MFCs reactors.

2.6. Construction of the MFCs

A clear 4 mm acrylic sheets were used to fabricate the MFC reactors used in this study. The acrylic sheets were cut with a laser to the indicated dimensions. The MFC base was made of three stacked pieces of 6.8 cm × 6.8 cm dimensions. The top and bottom were acrylic pieces of 3 cm × 2.5 cm dimensions. A cube with an inner dimension of 3 cm × 3 cm × 3 cm was made and placed on the reactor chassis. Thus, providing an anode compartment with a volume of 27 cm^3. A rectangular void was placed on the opening of the assembled structure to serve as a house for the air cathode. On top of the cathode, an aluminum mesh was placed, and an acrylic flange was used to secure it with nuts and bolts. The cells were equipped with connectors for refilling with relevant media. The surface area of the anode was 3.5 cm^2, while the surface area of the air cathode was 7.5 cm^2. The generated power by the MFC was, therefore, evaluated with a normalized cathode surface area. The features and components of the MFC used in this study are shown in Figure 1.

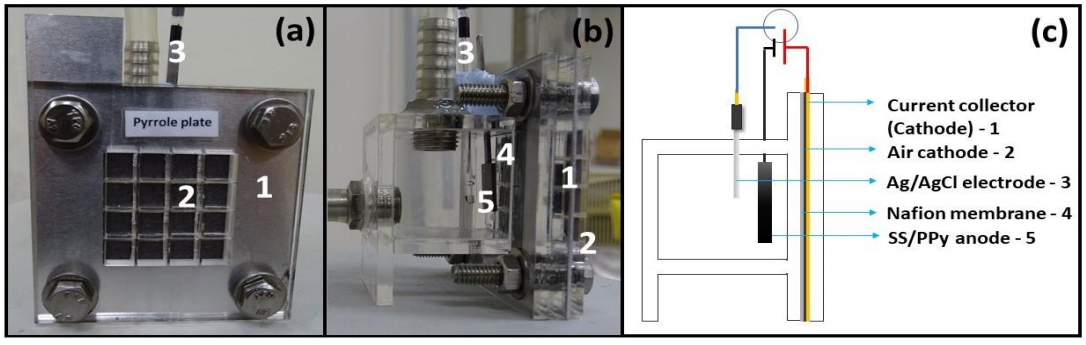

Figure 1. Features and components of the MFC explored in this study. (**a**) front view of MFC with air cathode window; (**b**) side view of MFCs showing all internal components; and (**c**) schematics of MFC.

2.7. Operation of the MFCs

Synthetic wastewater (M9 media), which contained sodium acetate (25 mM) as a carbon source, was fed to the MFCs. The M9 media per liter of deionized water contained 4.33 g Na_2HPO_4, 2.69 g $NaH_2PO_4.H_2O$, 0.13 g KCl, 0.31 g NH_4Cl, and 12.5 mL of each vitamin solution and trace metal [40,41]. We have previously demonstrated that landfill leachate is one of the most promising substrates for MFCs [42]. Thus, as a bacterial

source in the M9 media, 4% landfill leachate harvested from the landfill site (Suez Environment, Melbourne, Australia), was inoculated. All runs were performed at an ambient temperature of 25 ± 2 °C. The reactors were flushed with N_2 gas for 5 min, and the media were sparged with nitrogen gas for 30 min before inoculation to ensure removal of O_2 and, thus, reduce aerobic degradation of the M9 media. The tests were performed in a fed-batch mode. After each batch cycle, 90% of the M9 media was replaced with fresh M9 media. Initially, the MFCs were operated under open circuit mode for two cycles, and then a 100 Ω external resistor was applied to evaluate current generation after biofilm formation in the two successive cycles. To evaluate the reproducibility of the MFC operation, all experiments were conducted in triplicate. Also, as a control, one set of experiments was carried out with the M9 media but without the bacterial inoculum.

3. Results and Discussion

3.1. PPy Film Formation

The galvanostatic electropolymerization of Py on SS-P was carried out in tartaric acid solutions, which contained 0.1 M Py with the application of a constant current of 2.5 mA cm^{-2} for 15 min. The use of 0.1 to 0.4 M L-(+)-tartaric acid gave, as shown in Figure 2a, distinctly higher activation and stabilization potentials that gradually decreased with increasing tartaric acid concentration up to 0.4 M. In contrast, the use of 0.5–0.7 M L-(+)-tartaric acid gave much lower activation and stabilization potentials that are very close together, indicating that more conductive PPy films were formed within this concentration range. However, 0.7 M tartaric acid gave a PPy film with the lowest stabilization potential and, hence, the most conductive film. This tartaric concentration (0.7 M) was therefore chosen for further consideration.

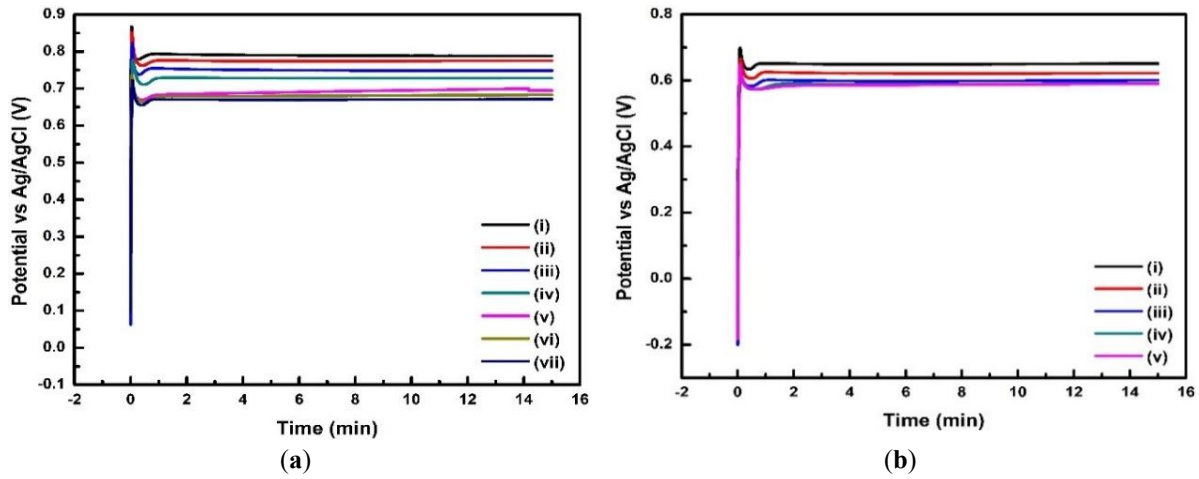

Figure 2. Chronopotentiograms obtained for the formation of PPy coatings on SS plates with (**a**) variable L-(+)-Tartaric acid concentration in the presence of 0.1 M Py and (**b**) varying Py concentration in the presence of 0.7 M L- (+)-Tartaric acid. L-(+)-Tartaric acid concentrations in (**a**), (i) 0.1M to vii 0.7 M, (**b**) (i) 0.1 to (v) 0.5 M Py concentration.

However, the conductivity of the PPy film can also be significantly influenced by the Py concentration used for the electropolymerisation. Figure 2b shows that the stabilisation potential of the PPy film decreased significantly with the use of increasing pyrrole concentration from 0.1 to 0.5 M. This was due to the increasing conductivity and thickness of PPy films formed on the SS-P. However, there was no notable difference between stabilisation potential obtained with 0.4 and 0.5 M Py. This suggests that identical PPy conductivity was obtained for films formed at either Py concentration. Based on this evaluation, a monomer solution that contained 0.4 Py and 0.7 ML-(+)-tartaric acid gave the most stable and conductive PPy coatings on the SS plate, as clearly demonstrated by the data in Table 1. This monomer composition was subsequently used for all other investigations.

Table 1. Optimal activation and stabilization potentials attained for PPy synthesis on the SS-P.

Acid/Salt	Concentration (M)	Py Concentration (M)	Activation Potential (E_a/V)	Stabilisation Potential (E_s/V)
L-(+)-tartaric acid	0.7	0.1	0.875	0.770
	0.7	0.2	0.776	0.708
	0.7	0.3	0.725	0.688
	0.7	0.4	0.704	0.658
	0.7	0.5	0.776	0.681

3.2. Characterization of PPy Coating

3.2.1. Fourier Transform Infrared Spectroscopy (FTIR)

The spectral changes caused by the presence of PPy film on the SS-P were investigated by FTIR. Figure 3a shows the spectra with a Gaussian deconvolution of the bands at 1733 cm^{-1} assigned to the free and site-specific interactions of the carbonyl group [43]. The strong band observed at 1658 cm^{-1} is related to the C=O stretch in the PPy film. The absorption peak at 1658 cm^{-1} was also due to a -C=O linkage in the PPy film. The C=O structure at the β-C of the pyrrole ring was typically due to the oxidation of PPy [44]. The bands at 1339 and 1069 cm^{-1} correspond to the =C-H in-plane vibrations, while the band at 828 cm^{-1} was due to the out-of-plane vibrations due to the polymerization of Py [45]. The band located at 951 cm^{-1} was associated with the C-H out-of-plane distortion of Py units. The peak at 796 cm^{-1} was due to the C–H out-of-plane ring deformation [46]. Based on the identification of the characteristic peaks, it was obvious that the presence of PPy coating on the SS-P [44] was confirmed by FTIR.

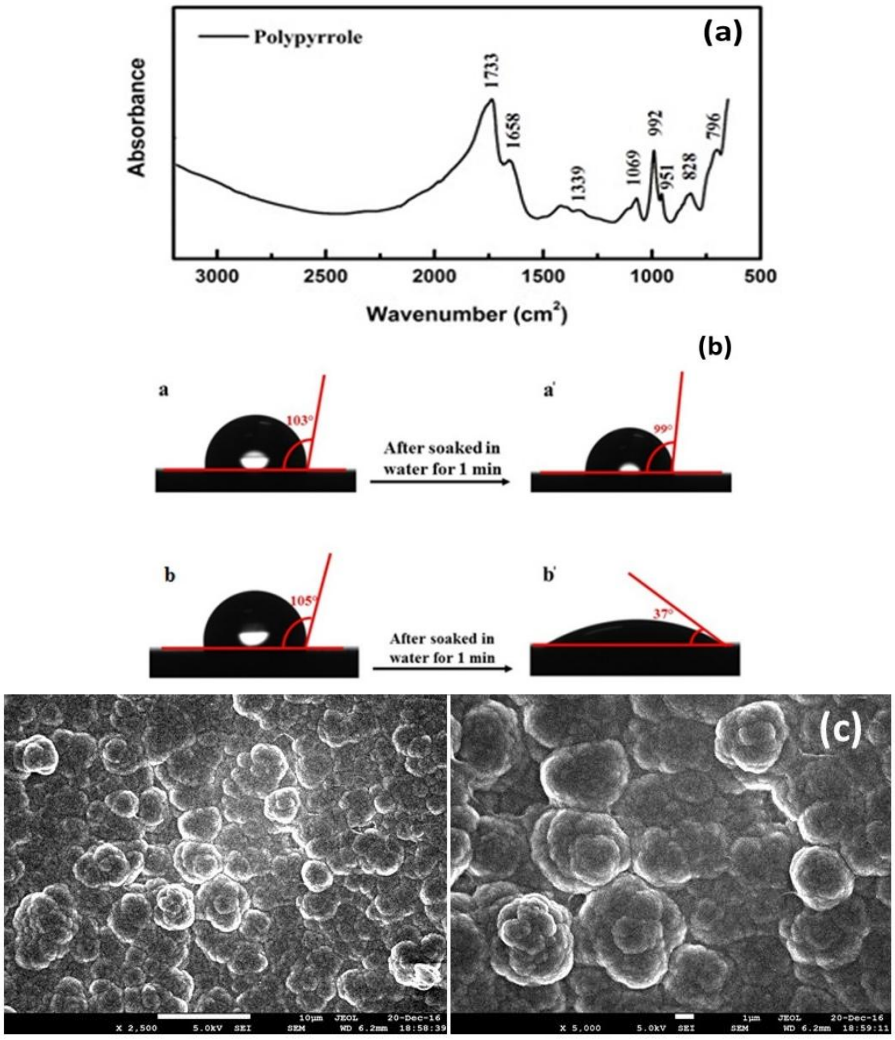

Figure 3. Characteristics of PPy films on pristine SS plate and PPy coated SS plate. (**a**) FTIR spectra of PPy film on SS-P; and (**b**) Contact angle measurement of (i, i`) SS-P and (ii, ii`) PPy/SS-P after soaking in water for 1 min; (**c**) SEM micrographs of PPy on SS-P.

3.2.2. Contact Angle Measurement and Scanning Electron Microscopy

Figure 3b illustrates the contact angle measurements of a pristine SS-P (a, a`) and PPy/SS-P (b,b`). The SS-P exhibited a hydrophobic surface (103°) and, notably, did not change after exposure to water (99°), remaining hydrophobic ($\theta > 90°$). In contrast, the contact angle for the PPy/SS-P was 105° (hydrophobic $\theta < 90°$), but reduced significantly to 37° (hydrophilic, $\theta \leq 90°$) after exposure to water. Evidently, the PPy/SS-P became hydrophilic when exposed to an aqueous medium. This will be particularly beneficial for its use as a MFC anode because the hydrophilic properties will tend to promote bacterial growth and adhesion, while the hydrophobic nature of the SS-P is undesirable

[15]. However, the wettability of a PPy coating is significantly reliant on several parameters, including the electrodeposition conditions, current density, the dopant, and the roughness of the film [47–49].

The morphology of the PPy-coated SS-P was also investigated by SEM. Figure 3c shows the presence of a compact cauliflower structure of the PPy at different magnifications. The compactness of the structure may render the surface of the SS-Ps protected, but when exposed to an aqueous medium, the PPy/SS-P will transition from a hydrophobic to a hydrophilic nature. The extent of surface protection it offers in this case will depend on the degree of retention of the surface coverage. If the surface remains fully covered in aqueous medium, PPy coating will give full protection and lower R_{ct}. However, if there are defects in the coatings, it will provide less protection and result in a small increase in R_{ct} due to the partial surface exposure.

3.3. Time-Dependent Electrochemical Spectroscopy

The use of electrochemical impedance spectroscopy was also explored for the evaluation of the PPy/SS-P, particularly in relation to the associated electrochemical reactions, coating stability, and coating kinetics [50,51]. Figure 4a shows the equivalent circuit (EC) R(Q(R(QR))) that was used to evaluate the EIS spectra and obtain the $R_{ct.}$ The EC is composed of solution resistance (R_s) combined in series with the lateral connection of the double-layer capacitor (*Cdl*) of the PPy film (Qc) and the polarization resistance (R_p). Subsequently, the R_p is associated with the parallel connection of the double-layer capacitor (*Cdl*) and the charge transfer resistance (R_{ct}).

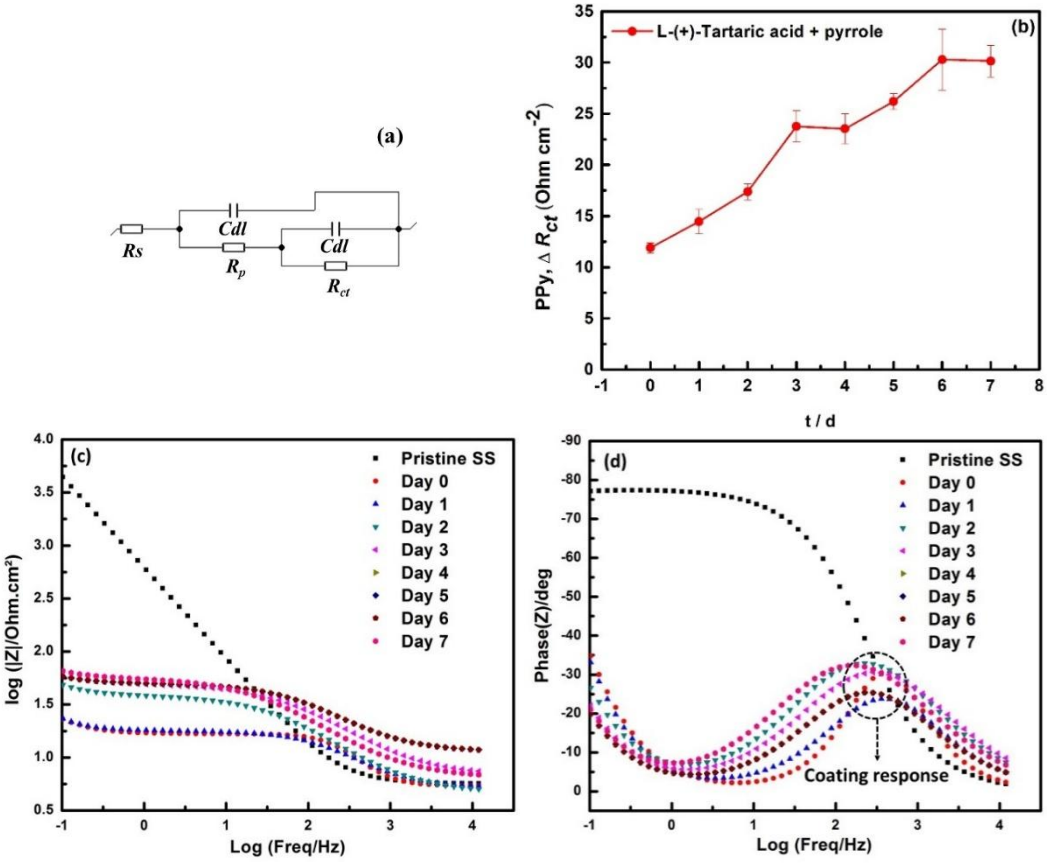

Figure 4. The analysis of PPy coating by longevity by time-dependent electrochemical spectroscopy; (**a**) equivalent circuit explored for EIS study; (**b**) alteration of PPy coating R_{ct} as a function of time in the corrosive solution; (**c**) frequency dependencies of the EIS and; (**d**) phase shift in the Bode plots of PPy coating.

To conduct the EIS measurements, the PPy/SS-P was immersed in 0.1 M NaCl solution at room temperature to enable measurement of the initial R_{ct} and subsequent monitoring of changes in R_{ct} in the corrosive medium over time. The samples were subjected, after every 24 h, to EIS measurements at varied scanning frequencies ranging between 1 MHz and 10 mHz. The EC lab software was used for data analysis and the equivalent circuit shown in Figure 4a was used to evaluate the R_{ct} of the system.

Figure 4b shows that the initial R_{ct} was low but increased slightly over time during the 7-day period. The small increases may be due to exposure of defective sites on the PPy coating. It also suggests that the ability of the PPy coating to protect the underlying SS-P decreased with time. Typically, the performance of an electrochemical

device is often adversely affected by a high charge transfer resistance, which typically signifies a barrier to electron transfer at the electrode-electrolyte interface [52,53]. More specifically, it indicates that the electrochemical reactions at the PPy coating/SS-P interface become increasingly difficult due to the coating degradation or formation of a resistive layer. Electrolytes and O_2 may penetrate the coatings via the defects/holes in the coatings to reach the underlying SS and, hence, result in the deterioration of the SS in the corrosive medium [55]. This can also be related to the tendency for the PPy/SS-P to transit from hydrophilic to hydrophobic nature, where the coating is defective, resulting in an increase in R_{ct} [15]. It is well known that the transition to the hydrophobic nature can hinder electron transfer and result in poor performance [25]. Hydrophilic surfaces achieve more efficient charge transfer due to their ability to enable easier movement of ions and interaction with the electrolyte. More specifically, the ease of formation of a biofilm on a hydrophilic surface lowers charge transfer resistance and promotes electron transfer between microorganisms and the anode surface, which in turn enhances MFC performance. In contrast, hydrophobic surfaces tend to hinder movement of ions, reduce interaction with the electrolyte and increase resistance [15]. However, it is important to note that despite the increase in the R_{ct} of the PPy/SS-P anode, the final value at around 30 Ohm cm^{-2} observed in this study is still relatively low and indicates that the coating still offered some protection.

More interestingly, the changes in the Bode plots (Figure 4d) revealed a distnct movement from a higher to lower phase with increasing frequency for the pristine SS-P over time. As the phase shift is related to the capacitive and resistive components of the steel's electrochemical behavior, the decline in the phase shift is reflective of the inability of the pristine SS-P to resist the penetration of the corrosive medium. In contrast, the Bode plot for the PPy/SS-P followed a peak-shaped response. The initial decrease in the phase shift in Bode plots obtained for the PPy/SS-P anode indicates a reduction in the coating's insulating or barrier properties. This implies that the coating became more conductive, permitting ions and molecules to pass through, possibly as a result of coating penetration caused by defects in the film where ions, O_2 and H_2O molecules were transferred across the coating [54]. But the phase shift increased as the coating became responsive on each of the 7 days at higher frequencies (log frequency of 0.5–2.5 Hz). Evidently, the effectiveness of the PPy coating decreased at lower frequencies where longer-term degradation mechanisms predominate [55,56]. Thus, indicating that the PPy coating provides higher insulating or barrier properties at high frequencies.

4. Performance of PPy/SS-P anode in Microbial Fuel Cells

The possible use of the PPy/SS-P and pristine SS-P as anodes for MFCs was investigated in M9 media with 25 mM acetate and 4% landfill leachate as a bacterial source [42]. In order to facilitate the establishment of biofilm on the anodes, two batch cycles were first conducted at room temperature without any external resistance. The SS-P anode gave maximum OCVs of 608 ± 32 mV and 664 ± 27 mV for the first and second cycles, respectively. In contrast, the PPy/SS-P anode gave maximum OCVs of 355 ± 33 mV and 624 ± 47 mV for the first and second cycles, respectively. Evidently, the first OCV obtained with the PPy/SS-P was much lower (253 mV less) than that obtained with the pristine SS-P, indicating that the presence of PPy coating was effective in lowering the initial OCV. This is consistent with the commonly held view that PPy coatings enhance the electrochemical properties of various electrodes [25]. Evidently, this observation is clearly reflective of the conductive nature of the coating on the PPy/SS-P anode, which reduced the internal resistance and lowered the OCV in the MFC. Although there was only a relatively small difference in the second OCVs obtained for both anodes, the OCV of the PPy/SS-P anode was still lower.

The trends of the OCVs with time for the two batch cycles are shown in Figure 5a. After two successive cycles, a fresh 25 mM sodium acetate was fed into the MFCs, and an external resistor of 100 Ω was connected to both systems. Notably, under these conditions, the MFC with the PPy/SS-P anode did not display a lag phase with the addition of the fresh sodium acetate solution. This observation is attributed to the successful biofilm formation on the PPy/SS-P anode during the initial two successive batch cycles conducted when no external resistance load was applied. Unlike the smooth surface of the SS-P anode that is not ideal for colonization by microorganisms, the coating of the SS-P with PPy (as PPy/SS-P anode) was beneficial in providing a rougher and a more porous surface with a larger area that was more amenable for colonization by microorganisms and aided the biofilm formation. As shown in Figure 5b, the MFC with the PPy/SS-P anode achieved a remarkably positive current generation on the first day due to its ability to better facilitate electron transfer from the bacteria to the electrode. A stationary current was observed during the current generation (~0.025 mA cm^{-2}) for three days. This is due to the stability and biocompatible nature of the PPy coating, which promotes the growth and adhesion of the microorganisms and consequently enables the maintenance of a stable and active biofilm on the PPy/SS-P anode. After the stationary phase, a sharp fall in current was observed on the fourth day of operation with the PPy/SS-P anode, possibly due to substrate depletion and generation of toxic substances from the bacterial

metabolic activities. Quite in contrast, the MFC with the SS-P anode generated much less current as evident in Figure 5b, producing only 0.012 ± 0.009 mA cm^{-2} on the first day. A slow decline was later observed for the remaining six days of operation. Thus, demonstrating that the use of the PPy/SS-P anode significantly lowered the startup time of the MFC, possibly due to the more efficient bacterial growth on the anode surface and the more efficient bacterial electron transfer to the electrode. The polarization curves obtained on the third day of the second batch cycle revealed, as shown in Figure 5c, that the SS-P anode gave a P_{max} of 0.010 ± 0.003 mW cm^{-2} under 0.027±0.0022 mA cm^{-2} current density normalized by the cathode area. On the other hand, the more efficient PPy/SS-P anode gave, as shown in Figure 5d, a much higher P_{max} of 0.020 ± 0.009 mW cm^{-2} under 0.070 ± 0.028 mA cm^{-2} normalized by the cathodic area. This was clearly due to the improved surface area, more efficient electron transfer and biocompatibility provided by the PPy coating. Table 2 summarises the comparative performances reported for polypyrrole-based anodes used for MFCs from previous studies, in terms of current and power densities. It is obvious that our PPy/SS-P anode area is significantly smaller than those used in most of the other studies. Nevertheless, in its initial use for MFC, the PPy/SS-P anode achieved slightly better maximum current density than the PPy/MnO_2 anode used in the Benthic MFC [37]. Also, its maximum power density was comparable to that obtained with PPy/CNTs anode [39], which had a much (3.5 times) larger surface area. It is therefore obvious from these observations that the use of a smaller anode did not affect the performance achieved with the PPy/SS-P anode. However, it is possible that by using a PPy/SS-P anode with a larger surface area further improvement in performance can be realised [22]. This aspect will be considered in a future study.

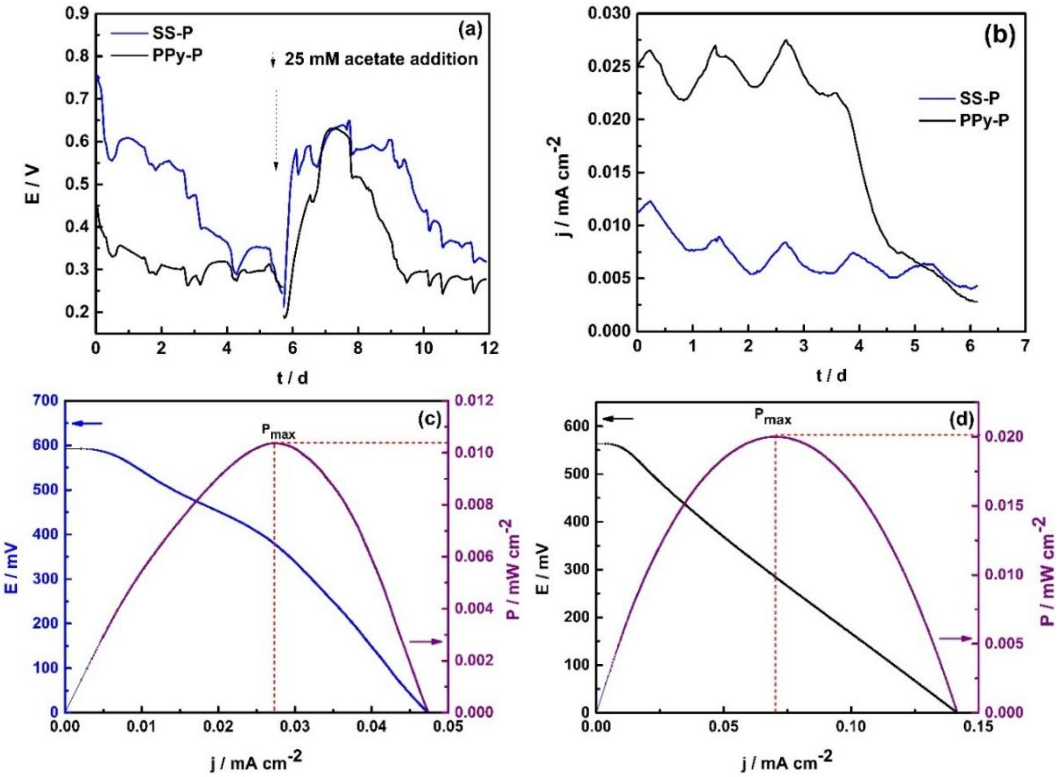

Figure 5. Bioelectrochemical performance of MFCs using pristine SS and SS modified with PPy anodes; (**a**) OCV of a system for two batch cycles; (**b**) current generation from MFC across 100 Ω resistor; (**c**) polarisation curve for SS-P anode system; (**d**) polarisation curve for PPy/SS-P anode system.

Table 2. Comparison of bioelectrocatalytic performance of PPy-modified anodes in MFCs.

Type of MFC	Vol. of Reactor (mL)	Anode Material	Anode Area (cm^{-2})	Max. Current Density (mA cm^{-2})	Max. Power Density (mW cm^{-2})	Reference
Dual chamber	0.5	PPy/RVC	0.0154	NA	1.200	[23]
H-shaped	10	PPy/CNTs	12.25	0.1278	0.0228	[39]
Single chamber	20	NT-MPMs	7	97000 †	32700 †	[57]
Benthic	NA	PPy/MnO_2	9	0.060	0.0562	[37]
Dual chamber	32	CPHs/CNTs	36.8	0.1600	0.1898	[24]
Single chamber	27	PPy/SS-P	3.5	0.070	0.020	Present work

† Volumetric power density (mW m^{-3}).

5. Conclusion

We have effectively demonstrated in this study that the inherent drawbacks in utilising SS for MFC can be addressed by applying a low-cost, long-lasting, and biocompatible PPy layer to the surface. This approach subsequently enabled the implementation of a high-performance MFC in a harsh, corrosive environment. Evidently, the success of this approach gave credence to the use of the established galvanostatic polymerisation conditions to produce PPy/SS-P anodes with low internal resistance, low OCVs, improved surface area, enhanced electron transfer and good biocompatibility for much improved MFC performance. The formation and presence of the PPy coating on the SS-P was successfully validated by FTIR measurements and the contact angle measurements revealed, for the first time, that the hydrophobic PPy coating transitioned to hydrophilic when immersed in aqueous solution, enabling the achievement of low OCVs and improved electrochemical performance. The PPy/SS-P anode subsequently gave an improved performance as an anode in MFC compared to a pristine SS-P anode. The optimized PPy/SS-P anode used in MFCs gave a P_{max} of 0.020 ± 0.009 mW cm^{-2} compared to a P_{max} of 0.010 ± 0.003 mW cm^{-2} obtained with the pristine SS-P anode. In particular, it was noted that the startup time of the MFC was significantly lowered with the use of the PPy/SS-P anode, which may be due to its biocompatibility and the ease of bacterial growth on the anode surface compared to the use of the pristine SS-P anode. Thus, demonstrating overall that the PPy coating was beneficial in improving the surface area, enhancing electron transfer and improving the biocompatibility of the PPy/SS-P anode. However, long-term performance studies are required and will be considered to further optimize the power generation obtained with the use of the PPy/SS-P anode in real wastewater.

Author Contributions

J.M.S.: conceptualization, methodology, data curation, writing—original draft preparation, and revision; I.K.: FTIR, R.K.S.: supervision; P.C.G.: Supervision; S.A.: conceptualization and re-conceptualization, methodology, resources, data analysis, writing—review & editing, supervision. All authors have read and agreed to the published version of the manuscript.

Funding

This research was funded internally by the Monash-IITB Academy.

Data Availability Statement

Not Applicable.

Conflicts of Interest

The authors declare no conflict of interest.

References

1. Sonawane, J.M.; Yadav, A.; Ghosh, P.C.; et al. Recent advances in the development and utilization of modern anode materials for high performance microbial fuel cells. *Biosens. Bioelectron.* **2017**, *90*, 558–576. https://doi.org/10.1016/j.bios.2016.10.014.
2. Santoro, C.; Arbizzani, C.; Erable, B.; et al. Microbial fuel cells: From fundamentals to applications. A review. *J. Power Sources* **2017**, *356*, 225–244. https://doi.org/10.1016/j.jpowsour.2017.03.109.
3. Sonawane, J.M.; Goenka, R.; Ghosh, P.C.; et al. Electrifying Waste Management: Integration of Polyaniline-Coated Electrodes in a Microbial Fuel Cell Stack for Power Generation and Leachate Treatment. *Environ. Sci. Technol.* **2023**, *57*, 6250–6260. https://doi.org/10.2139/SSRN.4600892.
4. Ucar, D.; Zhang, Y.; Angelidaki, I. An overview of electron acceptors in microbial fuel cells. *Front. Microbiol.* **2017**, *8*, 643. https://doi.org/10.3389/fmicb.2017.00643.
5. Hirooka, K.; Ichihashi, O.; Takeguchi, T. Sodium cobalt oxide as a non-platinum cathode catalyst for microbial fuel cells. *Sustain. Environ. Res.* **2018**, *28*, 322–325. https://doi.org/10.1016/j.serj.2018.07.002.
6. Baudler, A.; Schmidt, I.; Langner, M.; et al. Does it have to be carbon? Metal anodes in microbial fuel cells and related bioelectrochemical systems. *Energy Environ. Sci.* **2015**, *8*, 2048–2055. https://doi.org/10.1039/C5EE00866B.
7. Yuan, H.; He, Z. Graphene-modified electrodes for enhancing the performance of microbial fuel cells. *Nanoscale* **2015**, *7*, 7022–7029. https://doi.org/10.1039/c4nr05637j.
8. Peng, X.H.; Chu, X.Z.; Huang, P.F.; et al. Improved Power Performance of Activated Carbon Anode by Fe_2O_3 Addition in Microbial Fuel Cells. *Appl. Mech. Mater.* **2014**, *700*, 170–174. https://doi.org/10.4028/www.scientific.net/amm.700.170.

9. Wu, G.; Bao, H.; Xia, Z.; et al. Polypyrrole/sargassum activated carbon modified stainless-steel sponge as high-performance and low-cost bioanode for microbial fuel cells. *J. Power Sources* **2018**, *384*, 86–92. https://doi.org/10.1016/j.jpowsour.2018.02.045.
10. Mustakeem. Electrode materials for microbial fuel cells: Nanomaterial approach. *Mater. Renew. Sustain. Energy* **2015**, *4*, 22. https://doi.org/10.1007/s40243-015-0063-8.
11. Zhu, X.; Logan, B.E. Copper anode corrosion affects power generation in microbial fuel cells. *J. Chem. Technol. Biotechnol.* **2014**, *89*, 471–474.
12. Peng, X.; Chen, S.; Liu, L.; et al. Modified stainless steel for high performance and stable anode in microbial fuel cells. *Electrochim. Acta* **2016**, *194*, 246–252. https://doi.org/10.1016/j.electacta.2016.02.127.
13. He, Y.-R.; Xiao, X.; Li, W.-W.; et al. Enhanced electricity production from microbial fuel cells with plasma-modified carbon paper anode. *Phys. Chem. Chem. Phys.* **2012**, *14*, 9966–9971. https://doi.org/10.1039/c2cp40873b.
14. Mahadevan, A.; Gunawardena, D.A.; Fernando, S. Technology and Application of Microbial Fuel Cells. In *Technology and Application of Microbial Fuel Cells*; Bentham Science Publishers: Oak Park, IL, USA, 2014; pp. 13–32. https://doi.org/ 10.5772/57200.
15. e Silva, T.C.A.; Bhowmick, G.D.; Ghangrekar, M.M.; et al. SiOC-based polymer derived-ceramic porous anodes for microbial fuel cells. *Biochem. Eng. J.* **2019**, *148*, 29–36.
16. Cui, H.F.; Du, L.; Guo, P.B.; et al. Controlled modification of carbon nanotubes and polyaniline on macroporous graphite felt for high-performance microbial fuel cell anode. *J. Power Source* **2015**, *283*, 46–53.
17. Nosek, D.; Jachimowicz, P.; Cydzik-Kwiatkowska, A. Anode modification as an alternative approach to improve electricity generation in microbial fuel cells. *Energies* **2020**, *13*, 6596.
18. Kovendhan, M.; Kang, H.; Jeong, S.; Youn, J-S.; Oh, Park, Y-K.; Jeon, K-J. Study of stainless steel electrodes after electrochemical analysis in sea water condition, *Environmental Research* **2019**, *173*, 549–555.
19. Hou, J.; Liu, Z.; Yang, S.; et al. Three-dimensional macroporous anodes based on stainless steel fiber felt for high-performance microbial fuel cells. *J. Power Sources* **2014**, *258*, 204–209. https://doi.org/10.1016/j.jpowsour.2014.02.035.
20. Pocaznoi, D.; Calmet, A.; Etcheverry, L.; et al. Stainless steel is a promising electrode material for anodes of microbial fuel cells. *Energy Environ. Sci.* **2012**, *5*, 9645–9652. https://doi.org/10.1039/C2EE22429A.
21. Hou, J.; Liu, Z.; Li, Y. Polyaniline Modified Stainless Steel Fiber Felt for High-Performance Microbial Fuel Cell Anodes. *J. Clean Energy Technol.* **2015**, *3*, 165–169. https://doi.org/10.7763/JOCET.2015.V3.189.
22. Song, R.B.; Wu, Y.C.; Lin, Z.Q.; et al. Living and Conducting: Coating Individual Bacterial Cells with *In Situ* Formed Polypyrrole. *Angew. Chem. Int. Ed. Engl.* **2017**, *56*, 10516–10520. https://doi.org/10.1002/anie.201704729.
23. Yuan, Y.; Kim, S. Polypyrrole-coated reticulated vitreous carbon as anode in microbial fuel cell for higher energy output. *Bull. Korean Chem. Soc.* **2008**, *29*, 168–172. https://doi.org/10.5012/bkcs.2008.29.1.168.
24. Tang, X.; Li, H.; Du, Z.; et al. Conductive polypyrrole hydrogels and carbon nanotubes composite as an anode for microbial fuel cells. *RSC Adv.* **2015**, *5*, 50968–50974. https://doi.org/10.1039/C5RA06064H.
25. Kamali, S.; Esfandyari, M.; Jafari, D. A review of the application of polymeric materials in microbial fuel cells. *Polym. Bull.* 2025, 82:7465–7492.
26. Lin, X.Q.; Li, Z.L.; Liang, B.; et al. Identification of biofilm formation and exoelectrogenic population structure and function with graphene/polyanliline modified anode in microbial fuel cell. *Chemosphere* **2019**, *219*, 358–364.
27. Zhang, P.; Zhou, X.; Qi, R.; et al. Conductive polymer–exoelectrogen hybrid bioelectrode with improved biofilm formation and extracellular electron transport. *Adv. Electron. Mater.* **2019**, *5*, 1900320.
28. Kang, Y.L.; Pichiah, S.; Ibrahim, S. Facile reconstruction of microbial fuel cell (MFC) anode with enhanced exoelectrogens selection for intensified electricity generation. *Int. J. Hydrog. Energy* **2017**, *42*, 1661–1671.
29. Kumar, A.; Narayanan, S.S.; Thapa, B.S.; et al. Application of low-cost plant-derived carbon dots as a sustainable anode catalyst in microbial fuel cells for improved wastewater treatment and power output. *Catalysts* **2022**, *12*, 1580.
30. Sonawane, J.M.; Al-Saadi, S.; Raman, R.K.S.; et al. Exploring the use of polyaniline-modified stainless steel plates as low-cost, high-performance anodes for microbial fuel cells. *Electrochim. Acta* **2018**, *268*, 484–493. https://doi.org/10.1016/j.electacta. 2018. 01.163.
31. Sonawane, J.M.; Patil, S.A.; Ghosh, P.C.; et al. Low-cost stainless-steel wool anodes modified with polyaniline and polypyrrole for high-performance microbial fuel cells. *J. Power Sources* **2018**, *379*, 103–114. https://doi.org/10.1016/j.jpowsour.2018.01.001.
32. Pu, K.B.; Ma, Q.; Cai, W.F.; et al. Polypyrrole modified stainless steel as high performance anode of microbial fuel cell. *Biochem. Eng. J.* **2018**, *132*, 255–261.
33. Sonawane, J.M.; Ghosh, P.C.; Adeloju, S.B. Electrokinetic behaviour of conducting polymer modified stainless steel anodes during the enrichment phase in microbial fuel cells. *Electrochim. Acta* **2018**, *287*, 96–105. https://doi.org/10.1016/j.electacta.2018.07.077.

34. Gajda, I.; Greenman, J.; Ieropoulos, I.A. Recent advancements in real-world microbial fuel cell applications. *Curr. Opin. Electrochem.* **2018**, *11*, 78–83. https://doi.org/10.1016/j.coelec.2018.09.006.
35. Gnana Kumar, G.; Kirubaharan, C.J.; Udhayakumar, S.; et al. Synthesis, structural, and morphological characterizations of reduced graphene oxide-supported polypyrrole anode catalysts for improved microbial fuel cell performances. *ACS Sustain. Chem. Eng.* **2014**, *2*, 2283–2290. https://doi.org/10.1021/sc500244f.
36. Pérez-Rodríguez, P.; Ovando-Medina, V.M.; Martínez-Amador, S.Y.; et al. Bioanode of polyurethane/graphite/polypyrrole composite in microbial fuel cells. *Biotechnol. Bioprocess Eng.* **2016**, *21*, 305–313. https://doi.org/10.1007/s12257-015-0628-5.
37. Chen, W.; Liu, Z.; Su, G.; et al. Composite-modified anode by MnO 2 /polypyrrole in marine benthic microbial fuel cells and its electrochemical performance. *Int. J. Energy Res.* **2017**, *41*, 845–853. https://doi.org/10.1002/er.3674.
38. Roh, S.-H. Electricity Generation from Microbial Fuel Cell with Polypyrrole-Coated Carbon Nanofiber Composite. *J. Nanosci. Nanotechnol.* **2015**, *15*, 1700–1703.
39. Zou, Y.; Xiang, C.; Yang, L.; et al. A mediatorless microbial fuel cell using polypyrrole coated carbon nanotubes composite as anode material. *Int. J. Hydrog. Energy* **2008**, *33*, 4856–4862. https://doi.org/10.1016/j.ijhydene.2008.06.061.
40. Harnisch, F.; Koch, C.; Patil, S.A.; et al. Revealing the electrochemically driven selection in natural community derived microbial biofilms using flow-cytometry. *Energy Environ. Sci.* **2011**, *4*, 1265–1267. https://doi.org/10.1039/c0ee00605j.
41. Liu, Y.; Harnisch, F.; Fricke, K.; et al. Improvement of the anodic bioelectrocatalytic activity of mixed culture biofilms by a simple consecutive electrochemical selection procedure. *Biosens. Bioelectron.* **2008**, *24*, 1006–1011. https://doi.org/10.1016/j.bios.2008.08.001.
42. Sonawane, J.M.; Adeloju, S.B.; Ghosh, P.C. Landfill leachate: A promising substrate for microbial fuel cells. *Int. J. Hydrog. Energy* **2017**, *42*, 23794–23798. https://doi.org/10.1016/j.ijhydene.2017.03.137.
43. Ramoa, S.D.A.; Barra, G.M.O.; Merlini, C.; et al. Novel electrically conductive polyurethane/montmorillonite-polypyrrole nanocomposites. *Express Polym. Lett.* **2015**, *9*, 945–958.
44. Raotole, P.; Patil, P.P.; Gaikwad, A.B. Polypyrrole Coatings on Low Carbon Steel from Aqueous Oxalate Solution. *Int. J. Emerg. Technol. Adv. Eng.* **2013**, *3*, 62–67.
45. Vetter, C.A.; Gelling, V.J. Template-Free Aqueous Synthesis of Conductive Polymer Nanoparticles. US20140110636A1, 24 April 2014.
46. Li, Z.; Cai, J.; Cizek, P.; et al. A self-supported, flexible, binder-free pseudo-supercapacitor electrode material with high capacitance and cycling stability from hollow, capsular polypyrrole fibers. *J. Mater. Chem. A* **2015**, *3*, 16162–16167.
47. Chang, J.H.; Hunter, I.W. Characterization and control of the wettability of conducting polymer thin films. In Proceedings of the Materials Research Society Symposium, 31 January 2011; pp. 7–12. https://doi.org/10.1557/PROC-1228-KK04-03.
48. Thombare, J.V.; Lohar, G.M.; Shinde, S.K.; et al. Synthesis, characterization and surface wettability study of polypyrrole films: Effect of applied constant current density. *Electron. Mater. Lett.* **2015**, *11*, 266–270. https://doi.org/10.1007/s13391-014-4082-x.
49. Valtera, S.; Prokeš, J.; Kopecká, J.; et al. Dye-stimulated control of conducting polypyrrole morphology. *RSC Adv.* **2017**, *7*, 51495–51505. https://doi.org/10.1039/c7ra10027b.
50. Shen, X.; Xu, X.; Li, C.; et al. Robust coating for high-temperature and corrosion-resistant. *J. Vac. Sci. Technol. A* **2024**, *42*. https://doi.org/10.1116/6.0003954.
51. Goldoni, R.; Thomaz, D.V.; Ottolini, M.; et al. Characterization of *In situ* electrosynthesis of polyaniline on pencil graphite electrodes through electrochemical, spectroscopical and computational methods. *J. Mater. Sci.* **2024**, *59*, 10287–10308. https://doi.org/10.1007/S10853-024-09745-8.
52. Ha, P.T.; Moon, H.; Kim, B.H.; et al. Determination of charge transfer resistance and capacitance of microbial fuel cell through a transient response analysis of cell voltage. *Biosens.Bioelectron.* **2010**, *25*, 1629–1634.
53. Altahan, M.F.; Beltagi, A.M.; Abdel-Azzem, M.; et al. An impedimetric approach for determination of ammonium using silver/poly-1-aminoanthraquinone/carbon paste electrode. *Sci Rep.* **2024**, *14*, 18555. https://doi.org/10.1038/s41598-024-68321-x].
54. Ramesh, D. Evaluation of Corrosion Stability of Water Soluble Epoxy-Ester Primer through Electrochemical Studies. *Mater. Sci. Appl.* **2012**, *3*, 333–347.
55. Fan, C.; Liu, Y.; Yin, X.; et al. Electrochemical Behavior and Interfacial Delamination of a Polymer-Coated Galvanized Steel System in Acid Media. *ACS Omega* **2021**, *6*, 20331–20340. https://doi.org/10.1021/acsomega. 1c02270.
56. Zuo, Y.; Pang, R.; Li, W.; et al. The evaluation of coating performance by the variations of phase angles in middle and high frequency domains of EIS. *Corros. Sci.* **2008**, *50*, 3322–3328.
57. Yuan, H.; Deng, L.; Chen, Y.; et al. MnO_2/Polypyrrole/MnO_2 multi-walled-nanotube-modified anode for high-performance microbial fuel cells. *Electrochim. Acta* **2016**, *196*, 280–285. https://doi.org/10.1016/j.electacta.2016.02.183.